Davidson J., Wadhwa M., Hervig R., and Stephant A. (2020) Water on Mars: Insights from apatite in regolith breccia Northwest Africa 7034. *Earth and Planetary Science Letters* **552**, 116597.

# Water on Mars: Insights from apatite in regolith breccia Northwest Africa 7034

Jemma Davidson, Meenakshi Wadhwa, Richard L. Hervig, Alice Stephant

***Earth and Planetary Science Letters***
**Volume 552, 15 December 2020, 116597**

**Cite as:**

Davidson J., Wadhwa M., Hervig R., and Stephant A. (2020) Water on Mars: Insights from apatite in regolith breccia Northwest Africa 7034. *Earth and Planetary Science Letters* **552**, 116597.

https://doi.org/10.1016/j.epsl.2020.116597

## Supplementary Materials

## Appendix A

### Comparison of epoxy-mounted and anhydrously-prepared samples

During the course of this study we sought to further understand the effects on the H-isotope systematics and $H_2O$ concentrations of apatite in martian meteorites prepared via traditional hydrous methods (e.g., those used to prepare thin sections by mounting in epoxy and wet-polished, typically with water) versus those that were prepared anhydrously (i.e., dry-polished, mounted in indium metal). Data from two anhydrously-prepared indium mounts (IM1 and IM2) are discussed elsewhere in this paper. Here we compare this data with that collected from an epoxy mount (EM).

A comparison of epoxy-mounted and anhydrously-prepared pieces of the severely-shocked martian fall Tissint, a depleted shergottite, showed that the addition of terrestrial water affected phases to different degrees (Mane et al., 2016). The phosphate merrillite ($Ca_9NaMg[PO_4]_7$) and the silicate olivine ($[Fe,Mg]_2SiO_4$) were affected to a larger degree than the glassy phase maskelynite (similar composition to plagioclase series feldspar; $NaAlSi_3O_8$–$CaAl_2Si_2O_8$), which exhibited little to no effects. Merrilites in a polished, epoxy-mounted section had significantly higher $H_2O$ contents (2900–9600 ppm), compared to those in an anhydrously-prepared thick section (40–3800 ppm), while the H-isotopic compositions were affected by the isotopically light terrestrial water (δD values of –105–524 ‰ vs. 272–2418 ‰ in the epoxy-mounted section vs. the anhydrously-prepared thick section) (Mane et al., 2016).

Here we compare the phosphate apatite, specifically chlorapatite ($Ca_5[PO_4]_3[F,Cl,OH]$), in an epoxy-mounted (EM) section and in anhydrously-prepared, indium-mounted (IM) sections of the least-shocked martian meteorite NWA 7034. The EM apatite has higher $H_2O$ concentrations (858–10677 ppm vs. 796–8201 ppm) and isotopically lighter H (δD = –69–961 ‰ vs. 17–1164 ‰) than IM apatite; the difference is most apparent in matrix apatite (Fig. A3, Table A3). This is not surprising, since apatite in NWA 7034 contains microcracks (Fig. 1BDFH) and polishing in the presence of water and mounting in epoxy increases the potential for contamination by trapping or adsorbing water (at and possibly also below its surface). Nevertheless, the difference between NWA 7034 apatite in epoxy-mounted and anhydrously-prepared samples is smaller than seen in Tissint phosphate. This may be due to the enhanced fracturing of mineral grains in the more

shocked Tissint (~25–40 GPa) (Mane et al., 2016); the greater degree of fracturing would likely result in trapping more contamination by epoxy and fluids used during sample preparation. Since NWA 7034 is less shocked (5 to 15 GPa; Wittmann et al., 2015), its minerals presumably have fewer fractures and thus less potential for terrestrial contamination.

While it was not possible to locate portions of the same igneous clasts in the IM1 and EM sections due to their small size, a large apatite-bearing impact melt clast was identified in both of the adjacent thick sections. There is a significant difference between the apatite grain in this impact melt mounted in the IM1 section (apatite A1; $\delta D = 1081 \pm 18$ ‰; $H_2O = 1173 \pm 235$ ppm) and that mounted in the EM section (apatite E2; $\delta D = -69 \pm 8$ ‰; $H_2O = 10677 \pm 2135$ ppm), with the apatite in the epoxy mount (E2) having much higher water content and isotopically lighter hydrogen than the apatite in the anhydrously-prepared, indium mount (A1). As there is substantial variability in δD values and $H_2O$ contents within apatite grains from the same clasts in the anhydrously-prepared samples (Fig. A2A), it is unlikely that the analyzed portions of the apatite grain mounted in the IM1 and EM mounts had the same initial H-isotopic composition and $H_2O$ concentrations. However, due to shock-implantation during impact processing, the apatite in this clast is expected to have had higher δD values prior to sample preparation so the differences can be most likely be ascribed to contamination during polishing.

During traditional sample preparation, terrestrial contamination is introduced by fluids used during polishing and also by the epoxy in which they are mounted. One EM measurement sputtered into epoxy (monitored by imaging mass $^{12}C^{14}N$) that had infiltrated a micro-crack in the apatite grain; this analysis yielded a high $H_2O$ concentration (8510 ppm) and low δD (–42 ‰), demonstrating the effect of epoxy contamination on $H_2O$ concentrations and H-isotopic ratios.

All sample measurements of the H isotope compositions and water concentrations need to be corrected for the isotopic composition and abundance of the H background during analyses. As it was not possible to co-mount standards with the chip of NWA 7034 in the epoxy mount, the accuracy of the H isotope compositions and water abundances measured in apatites in the EM section may be questionable. In the case of the NWA 7034 EM section, which did not contain any co-mounted standards, the H background was

estimated via analysis of anhydrous phases (such as feldspar) in this sample assuming that the $H^-/O^-$ calibration remained consistent between mounts. However, it is possible that this is not the case and, therefore, we cannot conclusively state that the H isotopic systematics and the water contents of apatite from the EM section are robust. Since the anhydrously prepared samples (IM1 and IM2) were co-mounted with standards, background H was determined on the same mount as the unknown samples; this provides confidence that the analyzed abundance and isotopic ratio of the H background are robust and that the sample measurements can be appropriately corrected. Thus, the discussion in the main text focuses on the data obtained on the anhydrously-prepared IM samples, and not from the EM section.

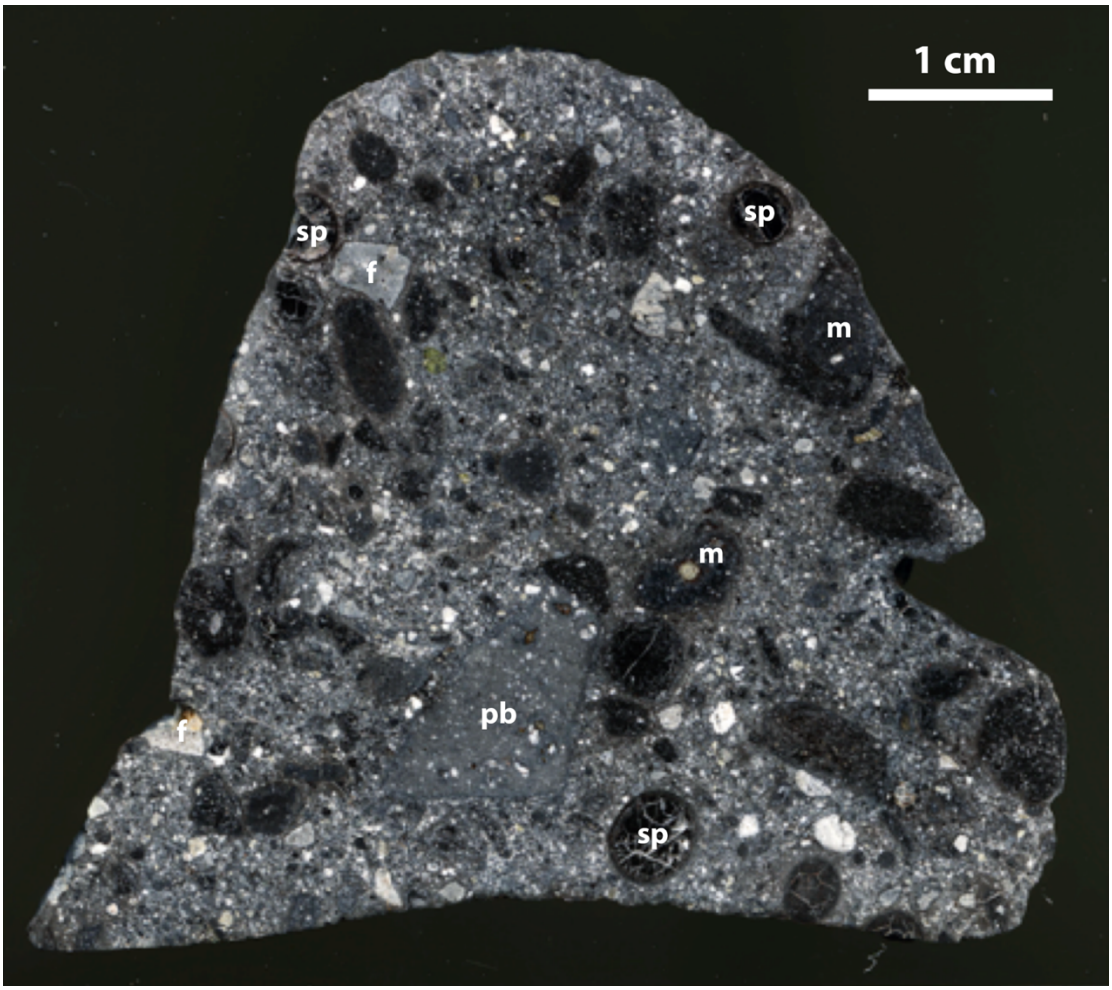


**Fig. A1.** Reflected light photograph of NWA 7034 material available in the ASU Center for Meteorite Studies collection prior to cutting. The brecciated nature of NWA 7034 is apparent in the numerous clasts, including dark rounded melt spherules (sp), melt clots (m), fine-grained proto-breccia clasts (pb), and light grey to white mineral fragments (f) in interclastic matrix. Labeled after Wittmann et al. (2015), with the exception of the proto-breccia clast (see Santos et al., 2015).

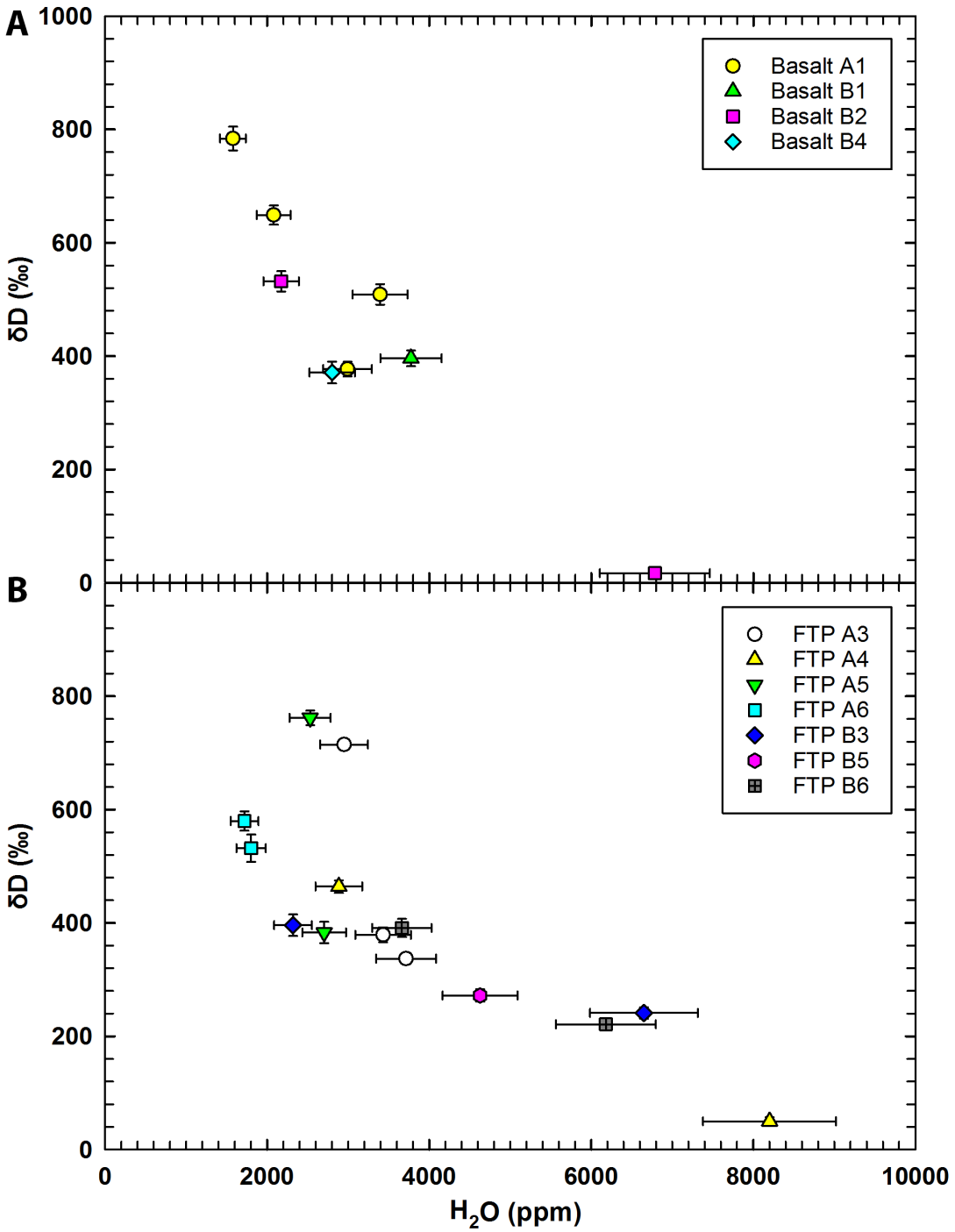


**Fig. A2.** H-isotopic composition versus water concentration in apatite from individual clasts. Data from anhydrously-prepared samples are broken down into (**A**) Basalt clasts, and (**B**) FTP clasts. Error bars represent 2σ uncertainties for δD (often smaller than the plotted symbols) and, for the sake of clarity, 1σ uncertainties for $H_2O$ concentrations.

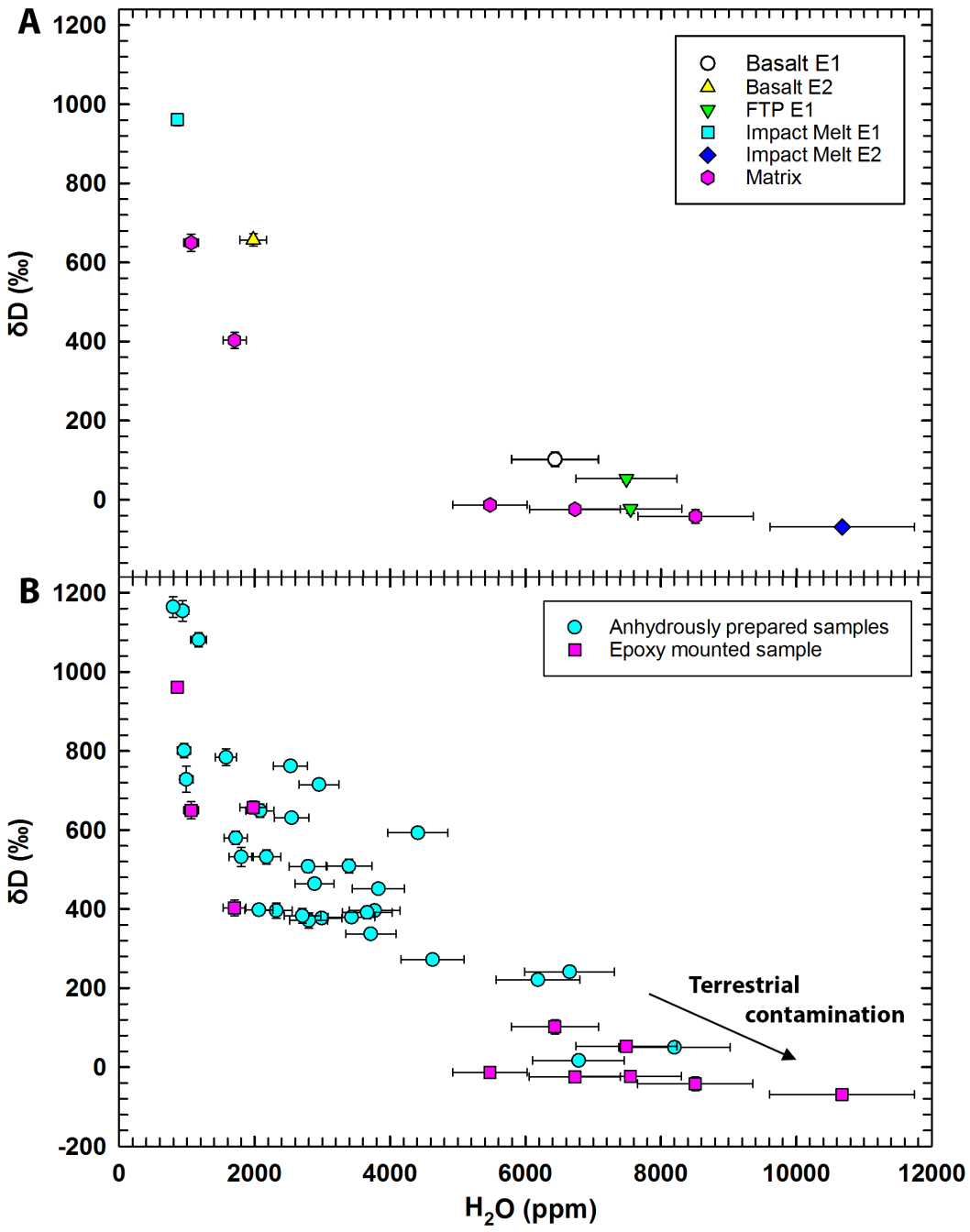


**Fig. A3.** H-isotopic composition versus water concentration in apatite from the epoxy-mounted NWA 7034. Data from the epoxy-mounted sample (**A**) grouped by lithological setting and (**B**) compared with anhydrously-prepared samples. Error bars represent 2σ uncertainties for δD (often smaller than the plotted symbols) and, for the sake of clarity, 1σ uncertainties for $H_2O$ concentrations.

**Table A1.** H-isotopic compositions (δD in ‰) and $H_2O$ concentrations (ppm) of the SIMS standards used in this study.

| Standard | Mineral | Source | δD (‰) | $H_2O$ (ppm) |
|---|---|---|---|---|
| Durango | Apatite | Mexico | –120 ± 5 | 600 |
| Macusani | Rhyolitic glass | Peru | –146 ± 8 | 3128 |
| P1326-2 | Basaltic glass | Juan de Fuca MORB | – | 2600 |
| PMR 53 | Clinopyroxene | South Africa | –101 ± 6 | 268 |
| PMR 53 dry | Clinopyroxene | Kimberlite | – | 0 |

Durango: Greenwood et al. (2008), McCubbin et al. (2012).
Macusani: Pichavant et al. (1987).
P1326-2: Dixon (1992).
PMR 53: Bell et al. (1995), Bell and Ihinger (2000).

**Table A2a.** Apatite elemental compositions. Data are shown (weight percent oxide) from both anhydrously-prepared and epoxy mounted samples. Data were corrected for F and Cl via the method of Ketcham (2015)*. Data for La and Ce are not shown as they were below detection limits (bdl) for every analysis. Water concentrations (weight percent $H_2O$) were calculated via stoichiometric difference.

| Clast/Matrix | Grain | CaO | $Na_2O$ | MgO | MnO | FeO | $SO_3$ | $Al_2O_3$ | $P_2O_5$ | $SiO_2$ | Cl | F | -O=F | -O=Cl | Total | OH (wt.%) |
|---|---|---|---|---|---|---|---|---|---|---|---|---|---|---|---|---|
| **Anhydrously-prepared samples** | | | | | | | | | | | | | | | | |
| Basalt A1 | 31 | 52.66 | 0.25 | 0.08 | bdl | 0.54 | 0.23 | 0.06 | 39.98 | 0.13 | 4.63 | 0.93 | 0.39 | 1.04 | 98.05 | 0.18 |
| Basalt A1 | 32 | 52.27 | 0.22 | bdl | bdl | 0.63 | 0.09 | bdl | 40.33 | 0.21 | 5.10 | 0.84 | 0.35 | 1.15 | 98.20 | 0.03 |
| Basalt A1 | 33 | 53.00 | 0.17 | 0.10 | bdl | 0.55 | 0.19 | bdl | 40.35 | 0.33 | 4.58 | 0.56 | 0.23 | 1.03 | 98.55 | 0.56 |
| Basalt A1 | 35 | 53.08 | 0.25 | bdl | bdl | 0.50 | 0.09 | bdl | 40.03 | 0.15 | 4.53 | 1.23 | 0.52 | 1.02 | 98.32 | –0.04 |
| Basalt B1 | 6 | 53.10 | 0.22 | 0.08 | 0.20 | 0.54 | 0.14 | 0.05 | 40.24 | 0.41 | 5.13 | 0.89 | 0.38 | 1.16 | 99.46 | 0.00 |
| Basalt B2 | 3 | 53.09 | 0.12 | 0.09 | bdl | 0.57 | bdl | bdl | 40.42 | 0.42 | 5.16 | 1.01 | 0.42 | 1.16 | 99.29 | –0.12 |
| Basalt B2 | 4 | 53.52 | 0.18 | bdl | bdl | 0.44 | bdl | bdl | 41.09 | 0.29 | 5.39 | 1.06 | 0.45 | 1.22 | 100.31 | –0.23 |
| Basalt B4 | 15 | 51.17 | 0.14 | 0.71 | bdl | 1.45 | 0.15 | 0.12 | 39.43 | 1.65 | 5.08 | 1.04 | 0.44 | 1.15 | 99.37 | –0.10 |
| FTP A3 | 10 | 52.73 | 0.17 | bdl | bdl | 0.21 | 0.15 | bdl | 40.86 | 0.22 | 5.31 | 0.93 | 0.39 | 1.20 | 98.99 | –0.12 |
| FTP A3 | 11 | 53.12 | 0.19 | bdl | bdl | 0.30 | bdl | bdl | 41.02 | 0.20 | 4.99 | 0.65 | 0.27 | 1.13 | 99.07 | 0.30 |
| FTP A4 | 13 | 53.26 | 0.15 | bdl | bdl | 0.42 | bdl | bdl | 40.81 | 0.28 | 4.16 | 1.40 | 0.59 | 0.94 | 98.95 | 0.03 |
| FTP A4 | 14 | 52.84 | 0.19 | 0.29 | bdl | 0.66 | 0.09 | bdl | 40.79 | 0.63 | 3.51 | 1.35 | 0.57 | 0.79 | 99.00 | 0.40 |
| FTP A5 | 4 | 52.23 | 0.26 | bdl | bdl | 0.62 | 0.10 | 0.05 | 40.97 | 0.20 | 5.15 | 0.98 | 0.41 | 1.16 | 98.99 | –0.08 |
| FTP A5 | 20 | 53.03 | 0.23 | bdl | bdl | 0.50 | bdl | bdl | 41.08 | 0.28 | 5.42 | 0.85 | 0.36 | 1.22 | 99.81 | –0.08 |
| FTP A6 | 27 | 55.36 | 0.15 | 0.07 | bdl | 0.45 | 0.09 | bdl | 39.75 | 0.68 | 5.14 | 1.09 | 0.46 | 1.16 | 101.16 | –0.14 |
| FTP A6 | 28 | 54.17 | 0.11 | bdl | bdl | 0.91 | 0.43 | 0.06 | 38.82 | 0.63 | 3.30 | 1.07 | 0.45 | 0.75 | 98.31 | 0.71 |
| FTP B3 | 12 | 52.72 | 0.18 | 0.07 | bdl | 0.54 | 0.10 | bdl | 40.54 | 0.40 | 5.39 | 1.16 | 0.49 | 1.22 | 99.39 | –0.36 |
| FTP B3 | 13 | 52.78 | 0.22 | bdl | 0.10 | 0.49 | 0.08 | bdl | 40.37 | 0.17 | 5.07 | 0.96 | 0.41 | 1.14 | 98.69 | –0.05 |
| FTP B5 | 18 | 52.72 | 0.19 | 0.07 | 0.14 | 1.01 | 0.17 | bdl | 40.19 | 0.39 | 5.28 | 1.04 | 0.44 | 1.19 | 99.57 | –0.20 |
| FTP B6 | 21 | 53.01 | 0.33 | 0.12 | bdl | 0.45 | 0.08 | bdl | 40.82 | 0.44 | 5.51 | 0.88 | 0.37 | 1.24 | 100.04 | –0.14 |
| FTP B6 | 22 | 53.03 | 0.20 | 0.23 | bdl | 0.48 | 0.22 | bdl | 39.74 | 0.59 | 5.31 | 0.97 | 0.41 | 1.20 | 99.15 | –0.16 |

**Table A2b.** Apatite elemental compositions (continued).

| Clast/Matrix | Grain | CaO | $Na_2O$ | MgO | MnO | FeO | $SO_3$ | $Al_2O_3$ | $P_2O_5$ | $SiO_2$ | Cl | F | -O=F | -O=Cl | Total | $H_2O$ (wt.%) |
|---|---|---|---|---|---|---|---|---|---|---|---|---|---|---|---|---|
| **Anhydrously-prepared samples** | | | | | | | | | | | | | | | | |
| Impact Melt | | | | | | | | | | | | | | | | |
| A1 | 1 | 52.92 | 0.15 | 0.00 | 0.11 | 0.32 | bdl | bdl | 40.75 | 0.15 | 4.56 | 0.97 | 0.41 | 1.03 | 98.50 | 0.20 |
| Matrix A1 | 16 | 52.80 | 0.27 | bdl | bdl | 0.48 | 0.08 | bdl | 41.42 | 0.11 | 3.97 | 0.65 | 0.27 | 0.90 | 98.73 | 0.80 |
| Matrix A2 | 16b | 52.94 | 0.19 | 0.08 | 0.11 | 0.80 | bdl | bdl | 40.55 | 0.29 | 4.88 | 1.29 | 0.54 | 1.10 | 99.49 | –0.23 |
| Matrix A3 | 22 | 52.80 | 0.21 | 0.06 | bdl | 0.41 | 0.12 | bdl | 41.24 | 0.09 | 4.53 | 0.99 | 0.42 | 1.02 | 99.00 | 0.22 |
| Matrix A4 | 78 | 52.62 | 0.18 | bdl | bdl | 1.01 | 0.15 | 0.05 | 40.13 | 0.33 | 5.12 | 1.20 | 0.50 | 1.15 | 99.13 | –0.28 |
| Matrix B1 | 1 | 52.78 | 0.19 | bdl | 0.11 | 0.24 | bdl | bdl | 40.98 | 0.25 | 4.76 | 0.96 | 0.41 | 1.07 | 98.78 | 0.12 |
| Matrix B2 | 2 | 53.14 | 0.20 | bdl | bdl | 0.37 | bdl | bdl | 40.95 | 0.14 | 5.46 | 1.05 | 0.44 | 1.23 | 99.63 | –0.29 |
| Matrix B10 | 10 | 52.67 | 0.22 | bdl | bdl | 0.63 | bdl | bdl | 40.62 | 0.22 | 5.36 | 1.01 | 0.43 | 1.21 | 99.09 | –0.22 |
| Matrix B11 | 11 | 52.92 | 0.18 | bdl | bdl | 0.42 | bdl | bdl | 41.08 | 0.09 | 5.36 | 1.05 | 0.44 | 1.21 | 99.44 | –0.24 |
| Matrix B23 | 23 | 53.11 | 0.19 | bdl | bdl | 0.18 | bdl | bdl | 40.60 | 0.24 | 5.37 | 0.82 | 0.34 | 1.21 | 98.95 | –0.05 |
| **Epoxy-mounted sample** | | | | | | | | | | | | | | | | |
| Basalt E1 | 34 | 53.50 | 0.13 | 0.10 | bdl | 0.57 | bdl | bdl | 41.34 | 0.20 | 2.47 | 1.80 | 0.76 | 0.56 | 98.79 | 0.51 |
| Basalt E2 | 36 | 53.02 | 0.18 | 0.18 | bdl | 0.61 | 0.12 | bdl | 40.40 | 0.54 | 4.71 | 0.77 | 0.32 | 1.06 | 99.13 | 0.33 |
| FTP E1 | 28 | 52.84 | 0.17 | bdl | bdl | 0.46 | 0.16 | bdl | 40.87 | 0.44 | 4.79 | 0.58 | 0.24 | 1.08 | 98.97 | 0.46 |
| FTP E1 | 29 | 53.18 | 0.21 | 0.06 | bdl | 0.61 | 0.11 | bdl | 41.65 | 0.35 | 5.75 | 1.09 | 0.46 | 1.30 | 101.25 | –0.39 |
| Matrix E1 | 23 | 52.59 | 0.20 | 0.20 | bdl | 1.69 | 0.08 | bdl | 40.86 | 0.49 | 3.63 | 0.78 | 0.33 | 0.82 | 99.36 | 0.85 |
| Matrix E2 | 24 | 51.83 | 0.36 | 0.19 | bdl | 1.06 | 0.21 | bdl | 40.69 | 0.36 | 5.42 | 1.08 | 0.45 | 1.22 | 99.52 | –0.29 |
| Matrix E3 | 26 | 52.87 | 0.20 | bdl | bdl | 0.60 | 0.19 | bdl | 41.47 | 0.15 | 4.31 | 0.94 | 0.39 | 0.97 | 99.36 | 0.39 |
| Matrix E4 | 31 | 52.36 | 0.20 | bdl | bdl | 1.25 | 0.10 | bdl | 40.43 | 0.25 | 4.93 | 1.12 | 0.47 | 1.11 | 99.06 | –0.11 |
| Matrix E5 | 33 | 53.01 | 0.17 | bdl | bdl | 1.20 | bdl | bdl | 40.74 | 0.20 | 5.00 | 0.89 | 0.37 | 1.13 | 99.71 | 0.08 |

*Data were processed using the "approach 1" template in Ketcham (2015).

**Table A3.** H-isotopic compositions (δD in ‰) and $H_2O$ concentrations (ppm) of apatite grains in various clastic lithologies from an epoxy-mounted sample of NWA 7034. Errors (2σ) associated with water concentrations are estimated to be ±20%.

| Clast/Matrix | Grain | δD (‰) | 2σ | $H_2O$ (ppm) | 2σ |
|---|---|---|---|---|---|
| Basalt E1 | 34 | 102 | 18 | 6435 | 1287 |
| Basalt E2 | 36 | 657 | 16 | 1979 | 396 |
| FTP E1 | 28 | 53 | 9 | 7489 | 1498 |
| FTP E1 | 29 | –23 | 11 | 7550 | 1510 |
| Impact Melt E1 | 40 | 961 | 15 | 858 | 172 |
| Impact Melt E2 | 42 | –69 | 8 | 10677 | 2135 |
| Matrix E1 | 23 | 403 | 20 | 1702 | 340 |
| Matrix E2 | 24 | 650 | 22 | 1061 | 212 |
| Matrix E3 | 26 | –13 | 13 | 5474 | 1095 |
| Matrix E4 | 31 | –24 | 10 | 6729 | 1346 |

**References**

Bell, D.R. Ihinger, P.D., 2000. The isotopic composition of hydrogen in nominally anhydrous mantle minerals. Geochim. Cosmochim. Acta 64 (12), 2109–2118.

Bell, D.R., Ihinger, P.D., Rossman, G. R., 1995. Quantitative analysis of trace OH in garnet and pyroxenes. Am. Mineral. 80, 465–474.

Dixon, J.E., 1992. Water and carbon dioxide in basaltic magmas. Ph.D. dissertation, California Institute of Technology.

Greenwood, J.P., Itoh, S., Sakamoto, N., Vicenzi, E.P., Yurimoto, H., 2008. Hydrogen isotope evidence for loss of water from Mars through time. Geophys. Res. Lett. 35, L05203.

McCubbin, F.M., Hauri, E.H., Elardo, S.M., Vander Kaaden, K.E., Wang, J., Shearer Jr., C.K., 2012. Hydrous melting of the martian mantle produced both depleted and enriched shergottites. Geology 40, 683–686.

Mane, P., Hervig, R., Wadhwa, M., Garvie, L.A.J., Balta, J.B., McSween Jr., H.Y., 2016. Hydrogen isotopic composition of the Martian mantle inferred from the newest Martian meteorite fall, Tissint. Meteorit. Planet. Sci. 51, 2073–2091.

Pichavant, M., Valencia Herrera, J., Boulmier, S., Briqueu, L., Joron, J.-L., Juteau, M., Marin, L., Michard, A., Sheppard, S. M. F., Treuil, M., Vernet, M., 1987. The Macusani glasses, SE Peru: Evidence of chemical fractionation in peraluminous magmas, in *Magmatic Processes: Physicochemical Principles*, B. O. Mysen, Ed. (The Geochemical Society, Washington, DC).

Davidson J., Wadhwa M., Hervig R., and Stephant A. (2020) Water on Mars: Insights from apatite in regolith breccia Northwest Africa 7034. *Earth and Planetary Science Letters* **552**, 116597.

Santos, A.R., Agee, C.B., McCubbin, F.M., Shearer, C.K., Burger, P.V., Tartèse, R., Anand, M., 2015. Petrology of igneous clasts in Northwest Africa 7034: Implications for the petrologic diversity of the martian crust. Geochim. Cosmochim. Acta 157, 56–85.

Wittmann, A., Korotev, R. L., Jolliff, B. L., Irving, A. J., Moser, D. E., Barker, I., Rumble III, D., 2015. Petrography and composition of Martian regolith breccia meteorite Northwest Africa 7475. Meteorit. Planet. Sci. 50, 326–352.